Supplementary Results.

Supplementary Figure 1. Backbone chemical shift changes plotted as a function of pH and fit to the Henderson-Hasselbalch equation to determine apparent pK_a values reported by the amide backbone ^{1}H and ^{15}N. For His106, the apparent pK_a value of 6.00 ± 0.02 obtained here is in good agreement with the value of 6.04 ± 0.06 determined previously from measuring side chain chemical shifts[1]. For the available reporters, we independently determined apparent pK_as for each $^{1H}\delta$ or $^{15N}\delta$ series from non-linear least-squares fits that use the Levenberg-Marquardt algorithm as installed in Igor Pro 6.1 (Wavemetrics, Oregon) to minimize χ^2, the goodness of fit. The modified Henderson-Hasselbalch equation can include up to three protonation events[2], and the number of ionization events for each $^{1H}\delta$ or $^{15N}\delta$ series was determined from χ^2 difference tests of nested models (based on a 95% confidence interval). In addition to intra-residue ionizations, some nuclei report on ionizations from non-adjacent but proximal residues that are ~10 Å or less (see Table 1 below).

a.

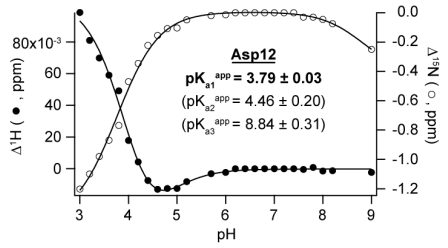

b.

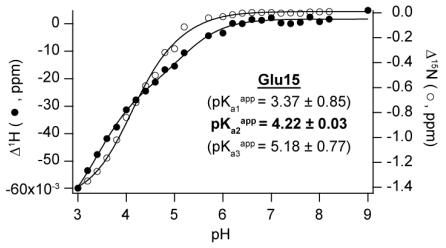

c.

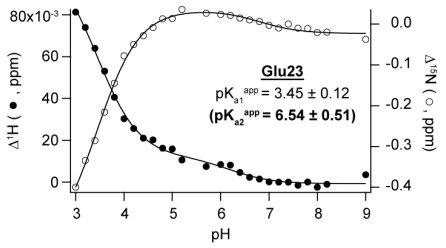

d.

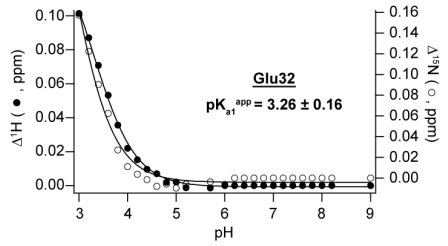

e.

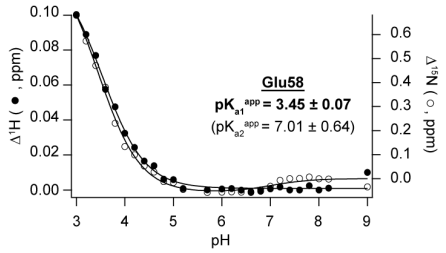

f.

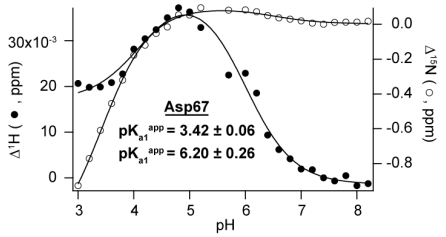

g.

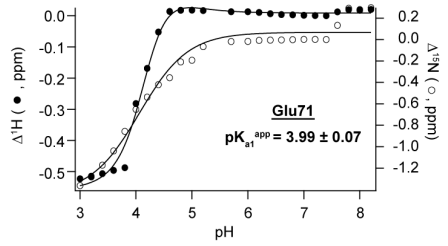

h.

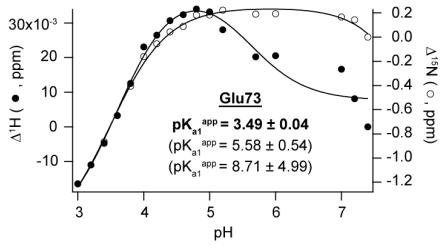

i.

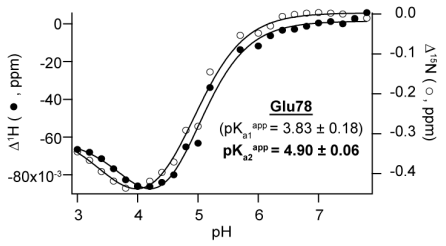

j.

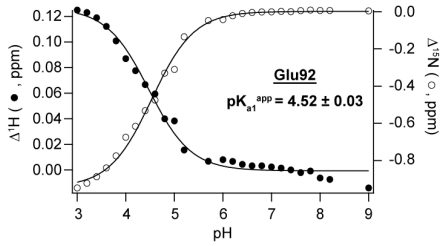

k.

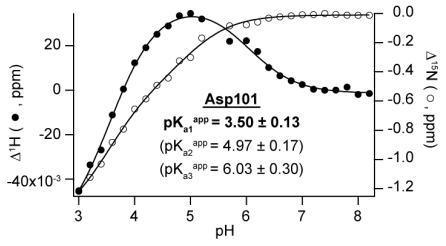

l.

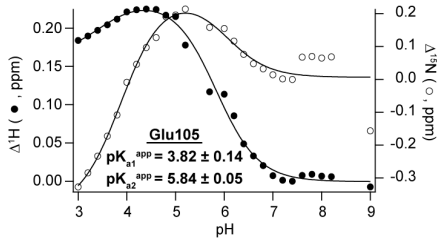

m.

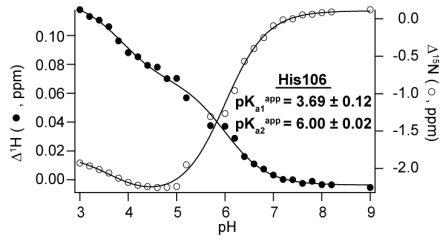

n.

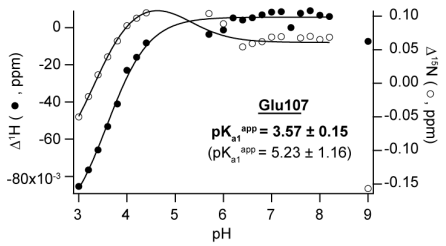

Supplementary Figure 2. The pK_a of Fis1-E78 is perturbed. To determine whether Fis1 pK_as were perturbed, we analyzed data presented in a compilation of previous studies[3], which reports an average apparent pK_a of 3.48 ± 1.08 and 4.22 ± 0.99 based on 138 and 152 measurements for Asp and Glu, respectively. These averages represent residues with perturbed sidechains (18 Asp and 20 Glu) that were either engineered or known to be involved in catalysis. Removing these perturbed values from the analysis, gives an average apparent pK_a of 3.38 ± 0.70 and 4.09 ± 0.64 based on 120 and 132 measurements for Asp (top panel) and Glu (bottom panel), respectively. The horizontal dashed line below represents ± 1 standard deviation. We used these "canonical" values to compare Fis1 Asp and Glu residues presented in Figure 1.

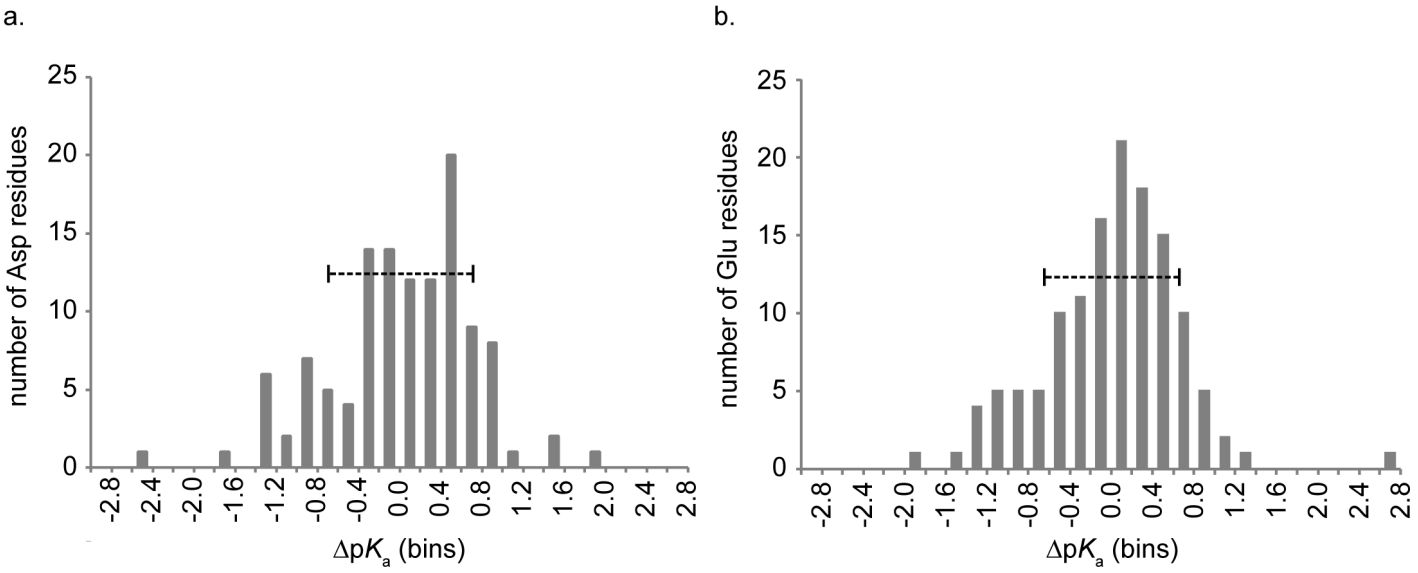

Supplemental Figure 3. Fis1 acidic residues with modestly elevated* pKa values (D12, E15, and E92 with ΔpK_a of 0.41, 0.13, and 0.43 respectively) are able to restore fission to WT levels *in vivo*. (a) WT or *fis1*Δ yeast transformed with mito-RFP and either empty vector, 1xHA-Fis1 WT or variants (D12A, E15A, or E92A) were grown to mid-log phase and plated on an agarose bed for imaging. Representative confocal image projections are shown. Scale bar represents 5 microns. (b) Mitochondrial morphology phenotypes from (a) were categorized into either WT or fission mutant. Using ImageJ, at least 100 cells were counted from 6 confocal image projections. Data represent the AVG ± STDEV from 3 independent experiments. Methods were identical to those described in Figure 2. *less that 1 standard deviation from the mean as shown in Figure 1 and Supplementary Figure 2.

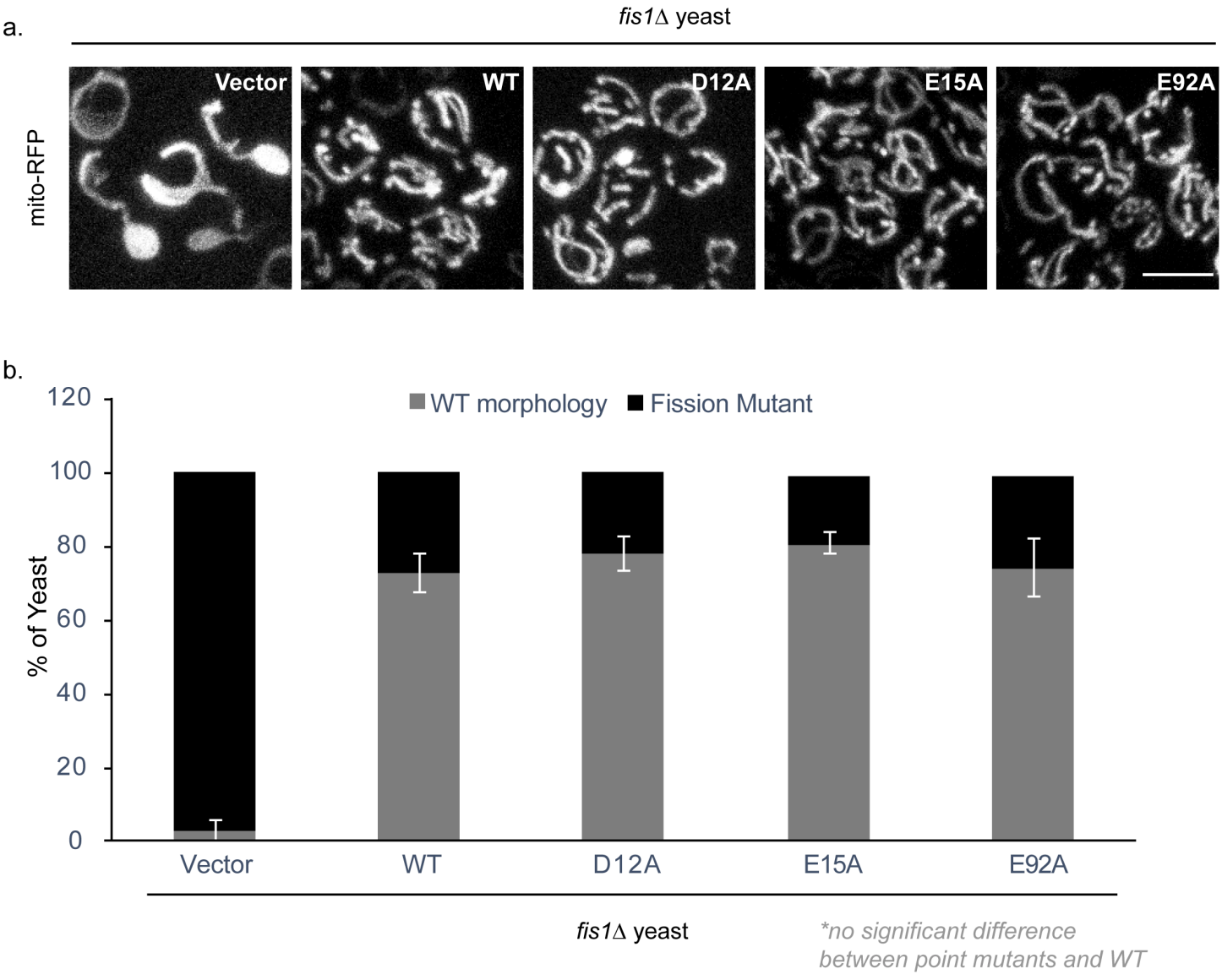

Supplementary Figure 4. The Fis1-E78A substitution does not affect structure, dynamics, folding, dimerization or membrane binding compared to WT Fis1. (a,b) Fis1-E78A retains a native-like fold as assessed by NMR. Superposition of ^{1}H-^{15}N HSQCs (a) were collected on 100 μ M ^{15}N-labeled Fis1ΔTM WT (black) or E78A (red) on a 500 MHz Bruker Avance III spectrometer equipped with a triple-resonance z-axis gradient cryoprobe at 25 °C in 90% H_2O/ 10% D_2O containing 20 mM HEPES pH 7.4, 175 mM NaCl, 2 mM DTT and 0.02% sodium azide. (**b**) The chemical shift perturbations (CSP; $^{1}H/^{15}N$ Δδ chemical shift) due to the E78A mutation was quantified for individual amino acid residues of WT Fis1, with substantial CSPs highlighted in blue (CSP ≥ 0.212 ppm) and mapped onto crystal structure (inset) of Fis1 (3O48.pdb). Increased shades of blue indicate larger CSPs. Note that the majority of CSPs are minimal with only significant changes localized to the E78A substitution, which indicates a minimal perturbation to Fis1 structure. (**c**) **E78A does not affect ^{1}H linewidths of Fis1 N-terminal arm residues.** The ^{1}H linewidths of well-resolved Fis1 N-terminal arm residues were measured for WT and E78A Fis1 (including the sidechain indole resonance of W7) indicating no change in dynamics of the Fis1 arm upon substitution of E78A. (**d) Fis1-E78A is well folded as indicated by no change in the midpoint of unfolding.** Fis1-E78A retains a native-like fold as assessed from chemical denaturation experiments performed by monitoring the intrinsic fluorescence of the two tryptophan residues in Fis1ΔTM, Trp7 and Trp47, as a function of increasing guanidine hydrochloride (GdnHCl) concentration at 25°C. The Trp emission at 330 nm was plotted as a function of GdnHCl concentration and fit to a two-state model using the method of Santoro and Bolen[5] with the following fit equation $f(x) = \{(y_f+m_fx)+(y_u+m_ux)*\exp[-(\Delta G+m_gx)/RT]\}/\{1+\exp[-(\Delta G+m_gx)/RT]\}$ to determine the midpoint of the unfolding transition , C_M. For WT $C_M = 2.37$ and for E78A $C_M = 2.41$. The free energy of unfolding is not reported as Fis1 unfolding is kinetically trapped[6]. **(e, f) E78A does not significantly affect Fis1 dimerization.** Refolding experiments of Fis1ΔTM WT (**left panel**) and E78A (**right panel**) at pH 7.0 to assess the effect of E78A on Fis1 dimerization. WT and E78A Fis1ΔTM-His were unfolded by dialysis into 6M GdnHCl buffer at 7.0, then refolded into buffer without denaturant. Refolded samples (dashed lines) were analyzed by size exclusion chromatography along with protein samples that were not refolded (solid lines). At the protein concentration used, WT Fis1ΔTM-His re-equilibrates into monomer (M) and dimer (D) populations upon refolding. For E78A we saw a similar redistribution into monomer and dimer species. (**g,h) E78A does not significantly affect Fis1 membrane binding.** Membrane binding experiments with Fis1ΔTM WT (**g**) and E78A (**h**) at pH 7.0 and pH 4.5 to assess the effect of E78A on Fis1 membrane binding. WT and E78A Fis1ΔTM-His were incubated with and without lipid vesicles containing 60:40:0.25 Br_4DSPC:DOPG:Rh-DOPE at pH 4.5 and pH 7.0. After incubation, the samples were spun to sediment vesicles. The amount of protein in the supernatant and the pellet was analyzed by SDS-PAGE and quantitated using ImageQuant. WT Fis1ΔTM-His binds lipid vesicles at pH 4.5 but not pH 7.0, similar to previous studies comparing pH 5.0 and 7.0[4]. The E78A mutant behaved like WT Fis1 in this assay and bound vesicles at lower pH, but not at neutral pH, suggesting that Glu78 is not involved in pH-dependent membrane binding.

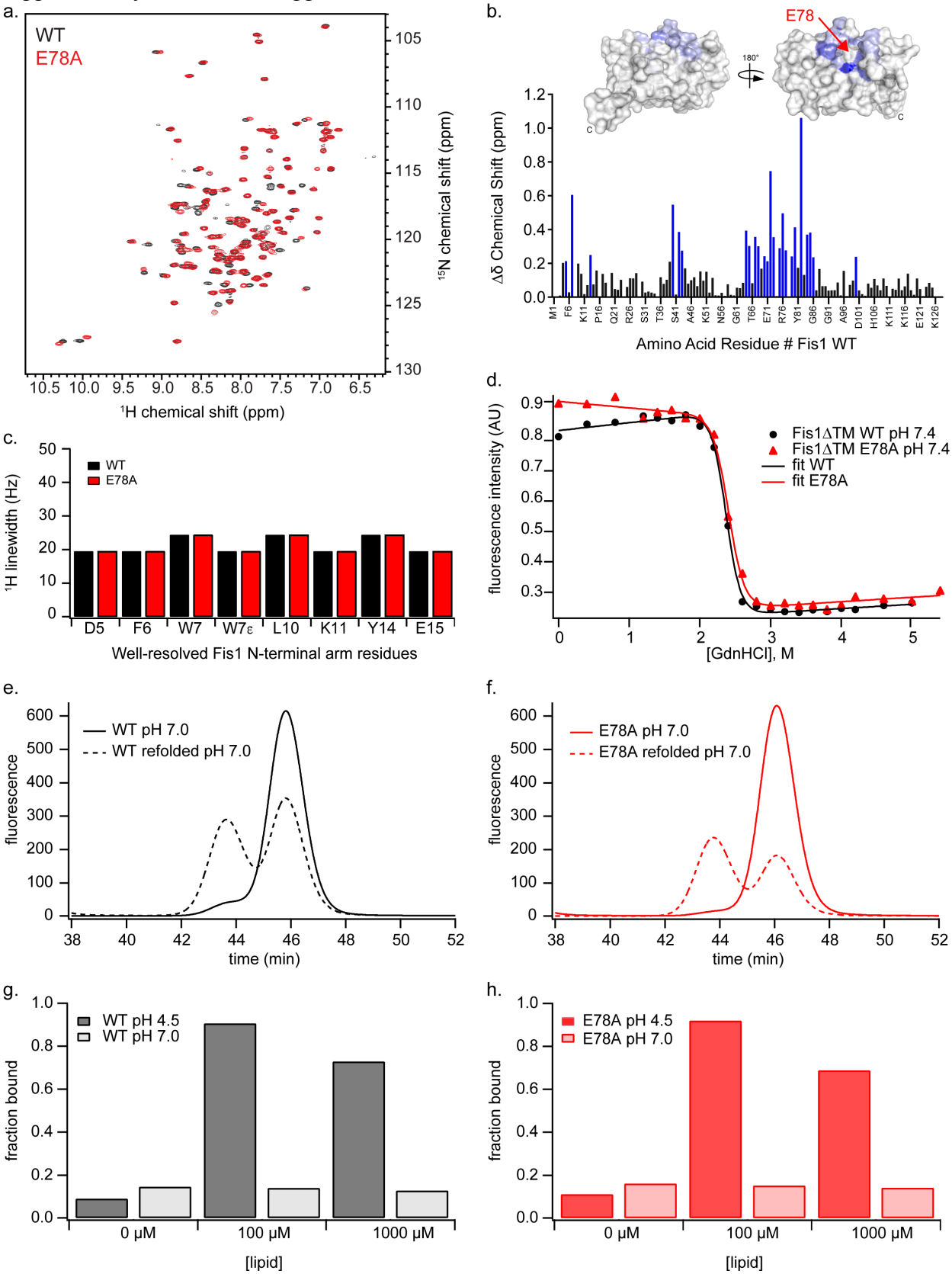

Supplementary Figure 4

Supplementary Figure 5. Possible physical basis for E78A disrupting the Fis1-Mdv1 or Fis1-Caf4 interaction. (**a**). In the complex with an Mdv1-derived peptide (cyan) bound to the concave surface of Fis1ΔTM[7] (grey), Fis1 Glu78 (yellow) receives a hydrogen bond from the Leu148 amide (2PQN.pdb). We predict substitution of Glu78 to Ala disrupts binding to Mdv1 by disrupting this hydrogen bond. (**b**) In the complex with a Caf4-derived peptide (purple) bound to the concave surface of Fis1ΔTM[7] (grey), Fis1 Glu78 (green) receives a hydrogen bond from the Leu126 amide (2PQR.pdb). We predict substitution of Glu78 to Ala disrupts binding to Caf4 by disrupting this hydrogen bond.

a.

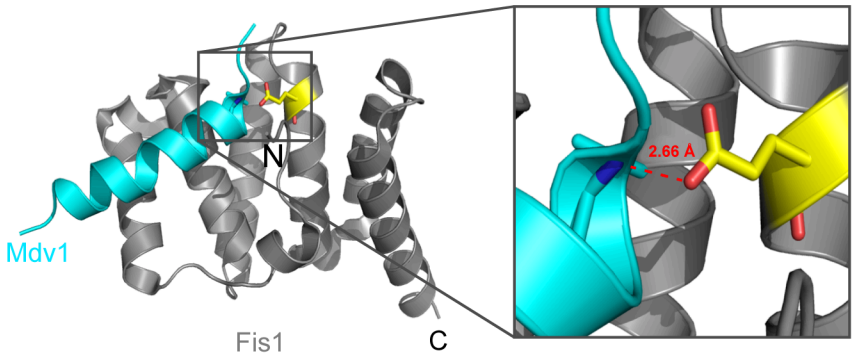

b.

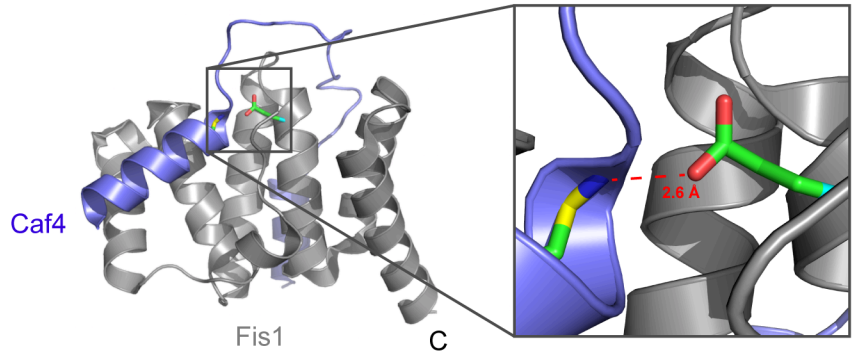

Supplementary Figure 6. Fis1-E78A does not bind Caf4 at WT levels. (**a**) Representative images from an anti-HA co-IP experiment using extracts from *fis1*Δ yeast expressing FLAG-Caf4 and either an empty vector, 1xHA Fis1 WT or E78A. (**b**) The results from (**a**) were quantified using ImageJ64 and were normalized to input. Data represents the AVG ± STDEV from 2 independent experiments.

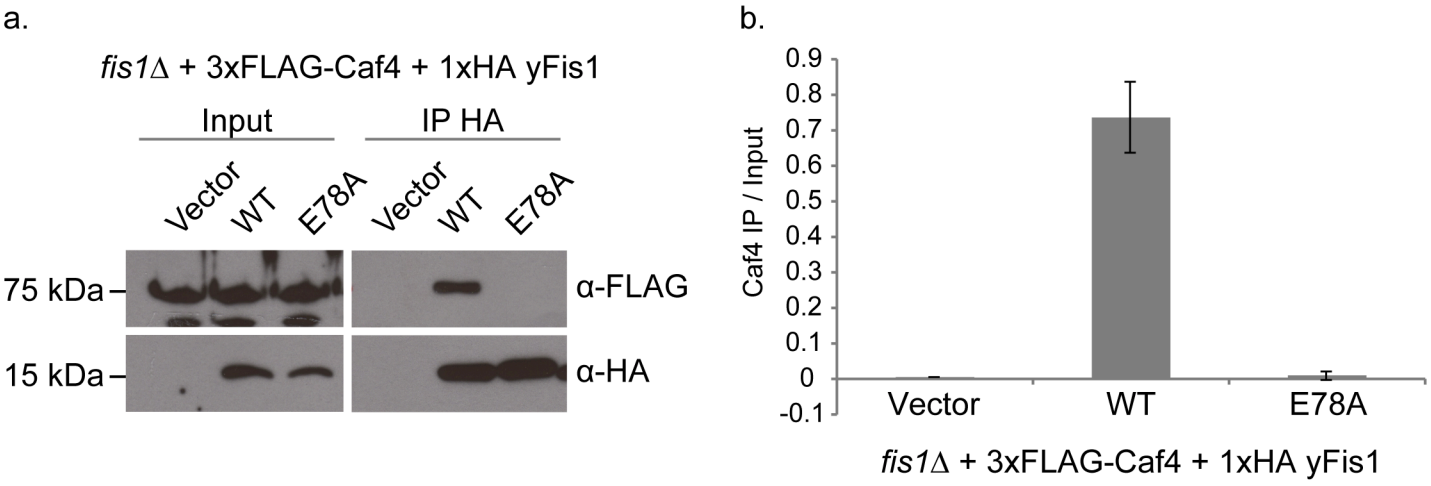

Supplementary Figure 7. Expression of Caf4 restores Dnm1 mitochondrial localization in a Fis1 dependent manner. (**a, c**) Representative confocal images from *fis1*Δ *mdv1*Δ *caf4*Δ expressing Dnm1-mCherry, mito-GFP, 3x-FLAG-Caf4 and either empty vector, 1X-HA-yFis1 WT, ΔN or E78A. The yeast were first grown overnight in media containing 5x MET and 2% Glucose (to suppress Caf4 and yFis1 expression, respectively) and then back-diluted into media containing 1x MET and 2% Galactose and grown for 3 hours to induce Mdv1 and yFis1 expression, respectively. Scale bar represents 5 microns. (**b**) Pearson's correlation co-localization index between Dnm1-mCherry and mito-GFP was determined from all cellular data from the 3 independent experiments from (**a**). Data is displayed as a scatter dot plot using Igor Pro and the mean value is indicated with the black line. ** denotes $p<0.01$ as assessed by ANOVA followed by TUKEY analysis.

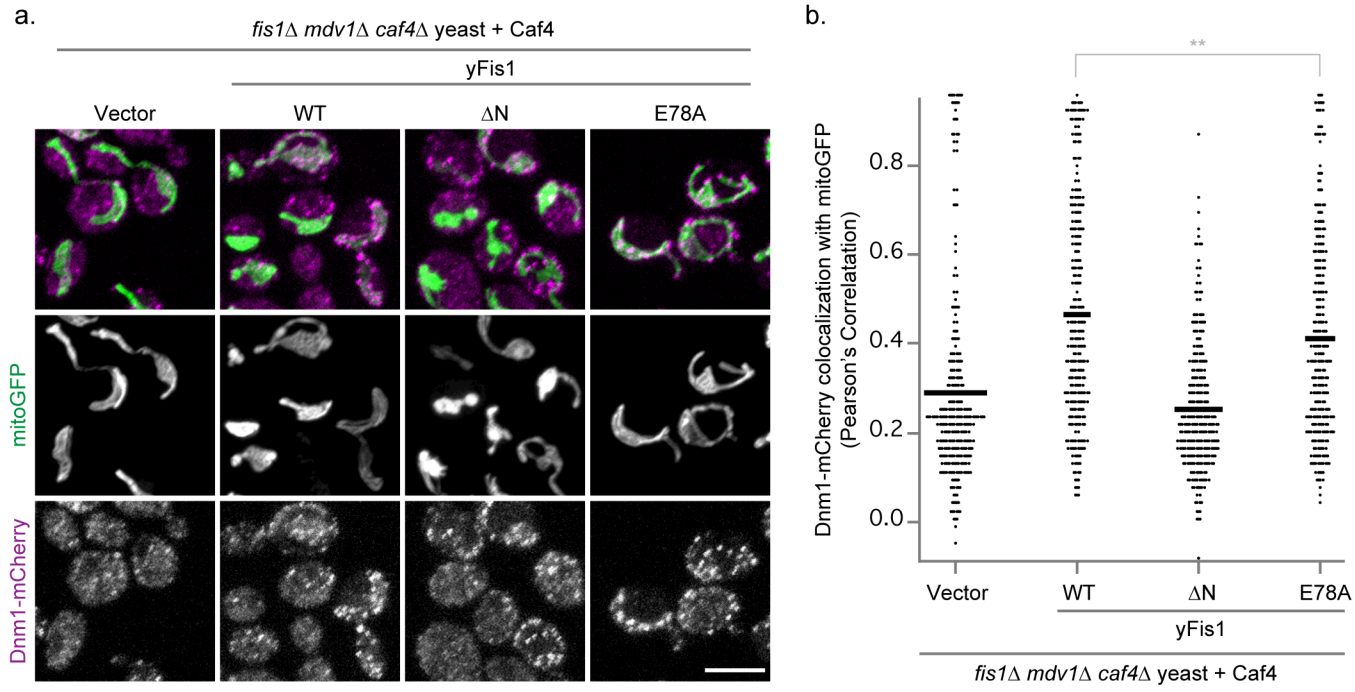

Supplementary Figure 8. Fis1-Mdv1 interfaces from crystallographic studies.
The structural data with a fragment of Mdv1 (cyan) in complex with Fis1 (green) shows stabilizing interactions in at least 3 sites (labeled Sites A, B, and C, derived from 3uux.pdb ref. 18). E78 lies at the Site B interface, leaving the other sites with the capacity to bind, but likely at a much weaker affinity (given the robust decline in both pull-down and coIP experiments, Main Figure 3). Whether these interactions are formed from a contiguous Mdv1 chain is not known: electron density is *not* observed for the Mdv1 polypeptide between the 3 sites (highlighted by a dashed red line and a question mark) raising the possibility that the stoichiometry of Fis1:Mdv1 is not 1:1.

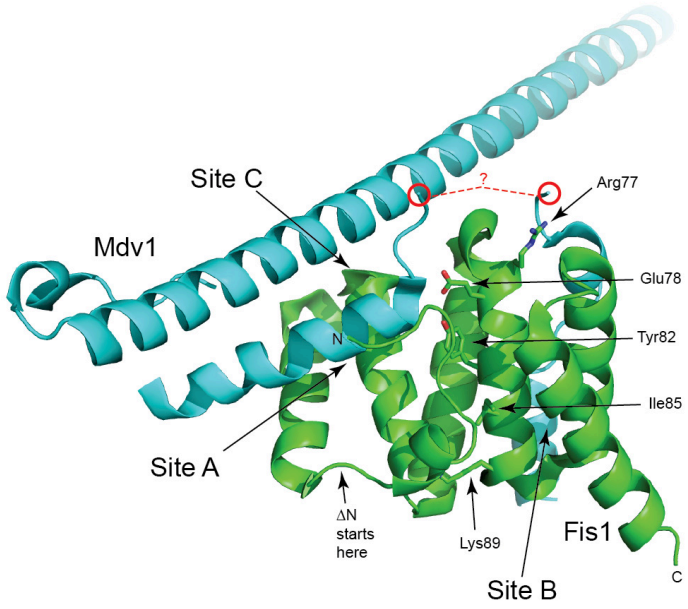

Supplementary Figure 9. Sequential model for assembly of the yeast fission machinery.
Fis1, Mdv1, and Dnm1 are essential for yeast mitochondrial fission. Fis1 is anchored to the mitochondrial outer member by a single-spanning transmembrane domain. In the absence of Fis1, Mdv1 and Dnm1 are primarily cytoplasmic. In the absence of Mdv1, Dnm1 is found primarily in punctate structures unless Caf4 is also deleted, which results in cytoplasmic localization. In the absence of Dnm1, Mdv1 is uniformly distributed on the mitochondrial surface presumably co-localized with Fis1. These data along with pairwise interaction data have led to a sequential model for yeast mitochondrial fission. Conflicting data exist as discussed in the main text.

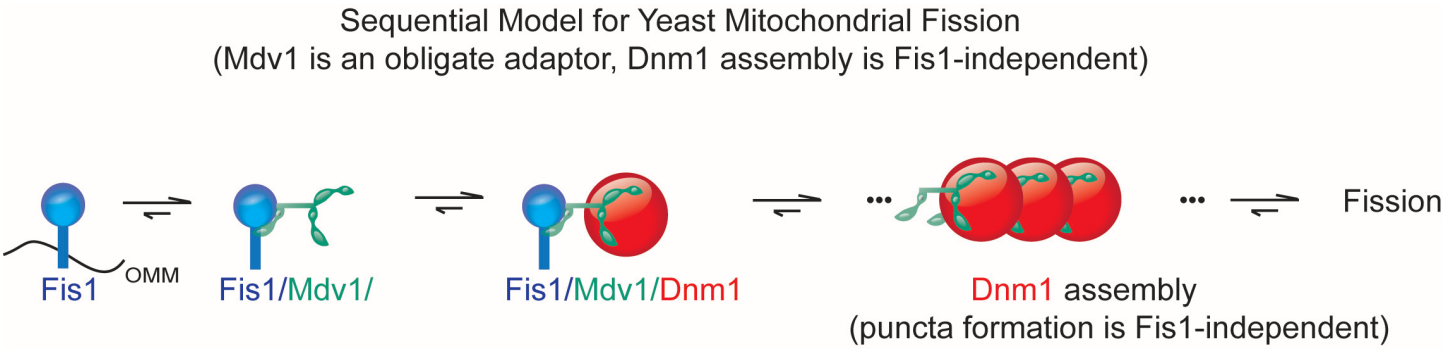

Supplemental methods

Assessment of pK_a values determined from pH-dependent chemical shifts.

Side chain protonation affects chemical shifts through space, thus the amide of an ionizable residue and its flanking residues in sequence – and potentially other amides nearby in space but not sequence – should report on the same apparent pK_a. 84 of the 126 Fis1 residues could be extracted to yield titration curves for pK_a analysis. The other peaks either did not show significant change in chemical shift during the titration or were in heavily overlapped regions of the spectrum preventing unambiguous assignment or accurate measurement of peak intensity. For each ionizable residue (*i*), we compared the apparent pK_as for its backbone amide $^{1H}\delta$ and $^{15N}\delta$ series with the adjacent residues (*i* - 1 and *i* + 1) and filtered for sets that were identical within experimental error[8]. Three acidic side chain pK_as (and the C terminus) are unassigned because appropriate backbone reporters are unresolved. Apparent pK_as sensed by some backbone reporters are not assigned to individual side chains because the backbone reporters are influenced by more than one nearby ionization event. Our assignments could be confirmed by pH titration experiments with double-mutant cycle analyses[9], but we verified many of them using a 1.75 Å Fis1 crystal structure[10] (3O48.pdb). Because the unique pK_a of the sole histidine of Fis1 (His106) is detected by backbone amide reporters up to 10 Å away, we classified backbone reporters by their distance from each ionizable group to confirm our assignments. Criteria similar to those proposed by Nielsen and co-workers[8] were applied, and only those pK_as that met all three conditions were considered "reliable":

1. Magnitude criteria

   $\Delta\delta \geq$ cutoff, where cutoff is 0.060 ppm for ^{1}H and 0.30 ppm for ^{15}N.

   This ensures that the magnitude of the chemical shift change is large enough to provide a good fit.

2. Uniqueness

   $pK_{a1}^{app} - pK_{a2}^{app} \geq 0.2$

   This criterion is for multiple pK_a fits and ensures that one is fitting distinct titration events.

3. Baselines

   $pK_a^{app} - pH_{min} \geq 0.25$; $pH_{max} - pK_a^{app} \geq 0.25$;

These ensure that reasonable pre- or post-transition baselines are present for fitting. In the absence of good baselines, an upper or lower limit to the pK_a can be determined.

All pK_as used to fit chemical shifts changes of backbone amides of ionizable residues, as depicted in the panels of Supplementary Figure 1, are reported in column 2 of Supplementary Table 1. Each of these pK_as is assessed according to reliability criteria (above), with results given in column 5. The pK_a assigned to the intra-residue side chain is given in **bold**. In two instances, D67 and E105, two reliable pK_as are detected on residue *i*. In both of these cases, the backbone reporters sense the intra-residue side chain ionization event as well as the ionization of H106, which is adjacent to E105. For D67, the *i*-1 reporter confirms the D67 pK_a but not the H106 pK_a, allowing us to confirm the D67 assignment without relying on structure. In two instances, D5 and D122, the intra-residue reporter is unresolved but a reliable pK_a from a residue adjacent in sequence is used to assign the side chain pK_a. These values are in italics, not bold, in column 2 and 3.

Uncertainties reported in the third column of Supplementary Table 1 are derived directly from fits to the data if only a single nucleus is reporting ("H" in column 4, or "N"), but if two nuclei report on the pK_a ("H,N" in column 4), the value and the error are the weighted averages of the pK_as from the two independent fits.

The intra-residue pK_as listed in bold in column 2 have been confirmed, in most instances, with values determined from adjacent residues (*i*-1 and *i*+1) that report on sidechain ionization[8]. In Supplementary Table 1, columns 7 and 8 list confirmatory pK_as obtained by fitting chemical shift data for residue *i*-1 and *i*+1 (respectively). Values and errors in columns 7 (or 8) represent the pK_as and reported errors from the fits (if a single reporter nucleus was used) or the weighted average and weighted error from two independent fits. In column 6, we indicate if the adjacent reporters help confirm the intra-residue apparent pK_a; if these secondary reporters confirm the pK_a, they are scored 'y'; if the proximity in sequence of another acidic side chain makes the confirmation ambiguous, they are scored 'a'. A lack of data is scored 'n'. Any reliability criterion that these confirmatory pK_as fail is identified by superscript.

In some cases, the ionization of a particular side chain is sensed by non-adjacent but 'dedicated' backbone reporters: in the crystal structure, these reporters are within 10 Å of only one particular acidic side chain, allowing the apparent pK_a to be assigned (if any is detected). A list of such reporters for each entry in Supplementary Table 1 is given in column 9, and

the average of all pK_as from these reporters is given in column 10. These values were not used in determining the pK_as reported in Fig 1b or Table 1.

More commonly, backbone reporters are close to more than one titratable side chain, and assigning the apparent pK_as would be more complicated. In the last column of Supplementary Table 1, we identify reporters that report on only two acidic side chains, but do not attempt to extract pK_as.

We estimated the maximum range at which an ionization can be directly detected by backbone reporters using His106, whose unique pK_a of 6.0 (determined earlier[1] and confirmed here) can be unambiguously assigned if detected on any backbone reporter. From analyzing all backbone reporters within 14 Å, we determined that reporters within 10 Å of an ionizable sidechain are potential reporters.

NMR Chemical Shift Perturbation and Linewidth Analysis of WT and E78A

Recombinant *S. cerevisiae* Fis1ΔTM$_{(1-128)}$ WT and E78A was produced using a pQE30 vector (kindly provided by Dr. B. Volkman) as an N-terminal His$_6$-Smt3-Fis1ΔTM$_{(1-128)}$ fusion construct that is cleavable by ubiquitin-like protease 1 (ULP1) and leaves an intact native N-terminus[11]. For protein expression, an overnight culture of *E. coli* pRep4 cells expressing His$_6$-Smt3-Fis1ΔTM$_{(1-128)}$ was grown and then used to inoculate 1 L of M9 minimal media containing 1 g/L $^{15}NH_4Cl$ containing kanamycin (30 μg/ml) and carbenicillin (30 μg/ml). Cells were grown at 37°C to an OD_{600} of ~1.2-1.3 and protein expression induced with 1 mM ispropyl β-D-1-thiogalactopyranoside (IPTG) at 18°C. After ~18 hours, cells were harvested and purified as described in protein expression and purification methods (main text) with the following exceptions. The column buffer was 20 mM HEPES pH 7.4, 175 mM NaCl, 30 mM imidazole, 0.02% sodium azide and bound protein was eluted with column buffer containing 500 mM imidazole. Affinity chromatography was performed with His60 Ni Superflow Resin (5 ml column, Clontech). The His$_6$-Smt3 affinity tag was cleaved by His$_6$-ULP1 overnight at 4°C in 20 mM HEPES pH 7.4, 175 mM NaCl, and 0.1% ß-mercaptoethanol. Cleaved Fis1ΔTM$_{(1-128)}$ was separated from the Smt3 affinity tag and ULP1 by a second affinity reverse-Ni chromatography step, which allowed cleaved Fis1 to flow through. Samples of 100 μM uniformly ^{15}N-labeled WT and E78A Fis1ΔTM$_{(1-128)}$ were used for NMR experiments to determine E78A-dependent chemical shift changes. NMR samples contained 20 mM HEPES pH 7.4, 175 mM NaCl, 2 mM DTT, 0.02% sodium azide, and 10% D_2O. ^1H-^{15}N heteronuclear single-quantum correlation (HSQC) experiments

were collected on a 500 MHz Bruker Avance III spectrometer equipped with a triple-resonance z-axis gradient Cryoprobe. NMR data were processed using NMRPipe (Ref 23 in main text). ^{1}H-^{15}N backbone assignments for Fis1 were determined previously[6] and validated against published solution structure assignments (1Y8M.pdb). ^{1}H-^{15}N HSQC overlays were constructed using the software XEASY[12] and Adobe Illustrator. ^{1}H linewidth analysis were performed on well-resolved yFis1 WT and E78A N-terminal arm residues using NMRDraw after processing without apodization (Ref 23 in main text).

Supplementary Table 1: Hierarchical assignment of apparent pK_as.

	from residue *i*				from residues *i*+1, *i*-1			from residues nearby in space (within 10 Å)		
residue	pK_a^{app}	error from fit	nuclei	reliable pK_a? (y/n)	confirm pK_a? (y/n/a)[7]	i-1 reporter pK_a^{app}	i+1 reporter pK_a^{app}	'dedicated' reporters: near one D/E	weighted average pK_a^{app}	'shared' reporters near more than one D or E (no pK_a estimates extracted)
D5				n[4]	y,n[4]	3.72 ± 0.09	unresolved	0		
D12	**3.79**	**0.04**	**H,N**	**y**	y,y[1]	3.45 ± 0.35	3.73 ± 1.30	0		4 (w/ E15): T9,L10
	4.46	0.2	H	n[1]						
	8.84	0.31	N	n[1,3]						
E15	3.37	0.85	H	n[1]						
	4.22	**0.03**	**N**	**y**	n[4],n[5]	unresolved	(Pro16)	0		4 (w/ D12): T9,L10
	5.18	0.77	H	n[1]						
E23	**3.45**	**0.12**	**H,N**	**y**	y,y	3.37 ± 0.14	3.36 ± 0.09	6: Q20,Q21,L25	3.75 ± 0.19	10 (w/ E32): R26,Q27,Q28, V29,V30
	6.6	0.51	H,N	n[1]						
E32	**3.26**	**0.16**	**H,N**	**y**	y,y	3.31 ± 0.07	3.39 ± 0.09	4: G34,S41	3.28 ± 0.07	10 (w/ E23): R26,Q27,Q28, V29,V30
D54	**3.34**	**0.05**	**H,N**	**y**	y,y	3.54 ± 0.11	3.20 ± 0.11	0		
	6.76	1.03	H	n[1]						
	7.97	0.17	N	n[1,3]						
D57	3.28	22.4	H	n[1,3]	y,a	3.51 ± 0.40	3.45 ± 0.07	0		
	8.7	0.23	H,N	n[1]						
E58	**3.45**	**0.07**	**H,N**	**y**	a[1,3],y	3.28 ± 22.4	3.62 ± 0.47	0		
	7.01	0.64	N	n[1]						
D67	**3.42**	**0.06**	**H,N**	**y**	y,n[4]	3.39 ± 0.21	unresolved	0		
	6.2	0.26	H,N	y	n,n[4]	(assigned to H106)				
E71	**3.99**	**0.07**	**H,N**	**y**	n[4],a[1]	unresolved	no xpks from 3-4.8	0		
E73	**3.49**	**0.04**	**H,N**	**y**	a[1],n[4]	no xpks	unresolved	0		
	5.58	0.54	H	n[1]						
	8.71	4.99	N	n[1]						
E78	3.83	0.18	H,N	n[1]						
	4.9	**0.06**	**H,N**	**y**	y[1],y[1]	5.47 ± 0.56	5.68 ± 1.58	2: L83	4.79 ± 0.67	4 (w/ E107): L80,Y81
E92	**4.52**	**0.03**	**H,N**	**y**	y,n[3]	4.39 ± 0.06	2.66 ± 2.93	1: T84	4.2 ± 0.2[6]	
D101	**3.5**	**0.13**	**H,N**	**y**	y,y	3.53 ± 0.19	3.58 ± 0.06	2: Y99	3.53 ± 0.03	
	4.97	0.17	N	n[1]						
	6.03	0.3	H	n[1]						
E105	**3.82**	**0.14**	**H,N**	**y**	y[1],a	3.83 ± 0.11	3.69 ± 0.12	0		
	5.84	0.05	H,N	y	y,y	(assigned to H106)				
H106	3.69	0.12	H,N	**y**	a[1],a[1]	E105/E107				
	6	**0.02**	**H,N**	**y**	y,y[1]	5.84 ± 0.05	5.23 ± 1.16	5:R77,T102, F104,R108	6.37 ± 0.19	
E107	**3.57**	**0.15**	**H,N**	**y**	a,y[1]	3.69 ± 0.12	3.52 ± 0.15	4: N110,Q112	3.69 ± 0.11	4 (w/ E78): L80,Y81
	5.23	1.16	N	n[1]						
E121	2.47	5.13	H	n[1,3]	n[4],a[4]	unresolved	unresolved	0		
D122				n[4]	a[4], y	2.47 ± 5.13	3.27 ± 0.37	0		
E127				n[4]	n[4], n[4]	unresolved	unresolved	0		

[1]Does not meet magnitude criteria; [2]Does not meet unique transition criteria; [3]Does not meet sufficient pre- or post-transition baseline criteria; [4]No NMR data because the resonance is unresolved; [5]No NMR data because the residue is proline; [6]Error from one site fit, not from averaging multiple reporters; [7]y=confirmed, n=not confirmed, a=ambiguous in that both i+1and i-1are ionizable.

Supplementary Table 2. Statistical Analyses.

Figure # (N; statistical test)	Sample	p-value	
Fig 2C (N=3 independent experiments; t-test)	WT yeast vs *fis1*Δ yeast (+ WT)	0.0014	**
	*fis1*Δ yeast: WT vs Vector	4.4E-06	***
	*fis1*Δ yeast: WT vs ΔN	4.2E-06	***
	*fis1*Δ yeast: WT vs E78A	0.00035	***
Figure 3b (N=3 independent experiments; t-test)	GST vs Fis1 WT	4.0E-06	***
	Fis1 WT vs Fis1 E78A	5.8E-06	***
Figure 3d (N=3 independent experiments; t-test)	Vector vs Fis1 WT	0.0091	**
	Fis1 WT vs Fis1 E78A	0.0090	**
Figure 3f (N=3 independent experiments; t-test)	GST vs Fis1 WT	0.24	n.s.
	Fis1 WT vs Fis1 E78A	0.031	*
Figure 3h (N=3 independent experiments; t-test)	Vector vs Fis1 WT	0.0061	**
	Fis1 WT vs Fis1 E78A	0.0061	**
Figure 4c (N= at least 162 individual yeast from 3 independent experiments; ANOVA followed by TUKEY)	WT yeast vs fis1 Δ yeast (vector)	3.5E-13	***
	WT yeast vs fis1 Δ yeast (+ WT)	9.9E-13	***
	WT yeast vs fis1 Δ yeast (+ E78A)	0.013	*
	*fis1*Δ yeast: vector vs WT	3.5E-13	***
	*fis1*Δ yeast: vector vs E78A	3.5E-13	***
	*fis1*Δ yeast: WT vs E78A	1.2E-10	***
Figure 4f (N= at least 164 individual yeast from 3 independent experiments; ANOVA followed by TUKEY)	WT yeast vs fis1 Δ yeast (vector)	0	***
	WT yeast vs fis1 Δ yeast (+ WT)	0.88	n.s.
	WT yeast vs fis1 Δ yeast (+ E78A)	0	***
	*fis1*Δ yeast: vector vs WT	0	***
	*fis1*Δ yeast: vector vs E78A	0	***
	*fis1*Δ yeast: WT vs E78A	0	***
Figure 5b (N= at least 265 individual yeast from 3 independent experiments; ANOVA followed by TUKEY)	Vector: vector vs WT	1.00	n.s.
	Vector: vector vs ΔN	0.99	n.s.
	Vector: vector vs E78A	0.90	n.s.
	Vector: WT vs ΔN	0.86	n.s.
	Vector: WT vs E78A	0.60	n.s.
	Vector: ΔN vs E78A	1.00	n.s.
	Mdv1: vector vs WT	0	***
	Mdv1: vector vs ΔN	0.97	n.s.
	Mdv1: vector vs E78A	0	***
	Mdv1: WT vs ΔN	0	***
	Mdv1: WT vs E78A	0	***
	Mdv1: ΔN vs E78A	0	***
	Vector::Mdv1: Vector vs Vector	0.95	n.s.
	Vector::Mdv1: WT vs WT	0	***
	Vector::Mdv1: ΔN vs ΔN	0.059	n.s.
	Vector::Mdv1: E78A vs E78A	0	***
Figure 6c (N= at least 71; ANOVA followed by TUKEY)	WT: 5X vs 1X	1.00	n.s.
	WT: 5X vs 0X	1.00	n.s.
	WT: 1X vs 0X	1.00	n.s.
	E78A: 5X vs 1X	0.38	n.s.
	E78A: 5X vs 0X	0	***
	E78A: 1X vs 0X	0	***
	WT::E78A: 5X vs 5X	0	***
	WT::E78A: 1X vs 1X	0	***
	WT::E78A: 0X vs 0X	0	***

The indicated statistical test, samples assessed and p-values are shown for the majority of comparisons for the main text figures. Statistical differences highlighted with blue are key comparisons, mainly regarding WT Fis1 versus Fis1 E78A.

Supplementary videos

Live cell imaging of the dynamic mitochondrial network. WT (video 1) or *fis1*Δ yeast co-expressing mito-RFP and either vector (video 2), 1xHA Fis1 WT (video 3), ΔN (video 4) or E78A (video 5) were grown overnight and back-diluted in media containing 1x MET. The yeast were then plated on an agarose imaging bed and imaged using an Olympus IX83 inverted microscope equipped with a DSU (Disk Scanning Unit) and a 100X OIL 1.4 UPlanSApo objective. Over the span of 17 minutes 60 images (each containing 15 slices with a step size of 0.5 microns) were acquired (1 image every ~17 seconds). Images were first processed into sequential projections using Metamorph and then using ImageJ64 and the TurboReg plugin minor XY drift was corrected.

Supplementary References

1. Picton, L., Casares, S., Monahan, A., Majumdar, A. & Hill, R. Evidence for conformational heterogeneity of fission protein Fis1 from Saccharomyces cerevisiae. *Biochemistry* **48**, 6598-6609, doi:10.1021/bi802221h (2009).
2. Shrager, R., Cohen, J., Heller, S., Sachs, D. & Schechter, A. Mathematical models for interacting groups in nuclear magnetic resonance titration curves. *Biochemistry* **11**, 541-547 (1972).
3. Grimsley, G. R., Scholtz, J. M. & Pace, C. N. A summary of the measured pK values of the ionizable groups in folded proteins. *Protein science : a publication of the Protein Society* **18**, 247-251, doi:10.1002/pro.19 (2009).
4. Wells, R. & Hill, R. The cytosolic domain of Fis1 binds and reversibly clusters lipid vesicles. *PloS one* **6**, doi:10.1371/journal.pone.0021384 (2011).
5. Santoro, M. M. & Bolen, D. W. Unfolding free energy changes determined by the linear extrapolation method. 1. Unfolding of phenylmethanesulfonyl alpha-chymotrypsin using different denaturants. *Biochemistry* **27**, 8063-8068 (1988).
6. Lees, J. P. *et al.* A designed point mutant in Fis1 disrupts dimerization and mitochondrial fission. *J Mol Biol* **423**, 143-158, doi:10.1016/j.jmb.2012.06.042 (2012).
7. Zhang, Y. & Chan, D. C. Structural basis for recruitment of mitochondrial fission complexes by Fis1. *Proceedings of the National Academy of Sciences of the United States of America* **104**, 18526-18530 (2007).
8. Farrell, D. *et al.* Titration_DB: storage and analysis of NMR-monitored protein pH titration curves. *Proteins* **78**, 843-857, doi:10.1002/prot.22611 (2010).
9. Fernández-Recio, J., Romero, A. & Sancho, J. Energetics of a hydrogen bond (charged and neutral) and of a cation-pi interaction in apoflavodoxin. *Journal of molecular biology* **290**, 319-330, doi:10.1006/jmbi.1999.2863 (1999).
10. Tooley, J. E. *et al.* The 1.75 A resolution structure of fission protein Fis1 from Saccharomyces cerevisiae reveals elusive interactions of the autoinhibitory domain. *Acta crystallographica. Section F, Structural biology and crystallization communications* **67**, 1310-1315, doi:10.1107/S1744309111029368 (2011).
11. Lee, C. D., Sun, H. C., Hu, S. M., Chiu, C. F., Homhuan, A., Liang, S. M., & Wang, T. F. (2008)). An improved SUMO fusion protein system for effective production of native proteins. Protein Science, 17(7), 1241-1248.).
12. Bartels, C., Xia, T.-H., Billeter, M., Güntert, P., and Wüthrich, K. (1995) The Program XEASY for Computer-Supported NMR Spectral Analysis of Biological Macromolecules. J. Biomol. NMR 6, 1−10.)